MINISTRY OF EDUCATION AND SCIENCE OF UKRAINE
NATIONAL TECHNICAL UNIVERSITY OF UKRAINE “IGOR SIKORSKY KYIV POLYTECHNIC INSTITUTE”

INSTITUTE OF AEROSPACE TECHNOLOGIES

Intelligence. Integration. Reliability

XIII international students and young scientists conference 9th December 2020

Kyiv
NTUU "Igor Sikorsky Kyiv Polytechnic Institute"
2020

CONTENTS

UDC 629.735.3

Burenin A. Nechyporenko O.

INCREASING THE QUADCOPTER RELIABILITY BY IMPROVING ITS AUTOMATIC CONTROL SYSTEM

Introduction. One of the urgent challenges is to ensure reliability during the design, production and exploitation of unmanned aerial vehicles (UAV) such as multicopters (quadcopters, copters). It is also important to increase the reliability of quadcopters at all stages of *flight*, which should be taken into account already at the design stage. In today's world, the role of the quadcopter is very large, it is used in various fields, but generally belongs to the objects of single use, including due to its low reliability.

Perfection the quadcopter automatic control system (ACS) in terms of increasing its functional reliability, developing a method of ranking of internal and external factors affecting the functional reliability of a quadcopter, taking into account the main sources of failures and influences on the ACS reliability and developing algorithm in general on their basis by using software redundancy according to the developed algorithm.

Scientific and technical results. During the design, a method of ranking internal and external factors influencing the reliability of the quadcopter and its ACS by the criterion of statistical assessment of the probability of failure of each component of the quadcopter was developed, ranked by the developed method, analysis of which allowed to identify weaknesses. According to this method, the algorithm of the additional computational program for the operation of the ACS of the quadcopter is designed, which is a software redundancy in terms of increasing functional reliability. The algorithm includes additional software actions in case of failure of one of the onboard navigation systems, detection of problems with the onboard computer, disconnection in flight of any of the propeller groups (use of bicopter model), disappearance of control signal from remote control during the flight behind an obstacle, software redundancy of the control circuit, etc.

Practical implementation. The use of the designed additional computing program in the quadcopter ACS the according to the developed algorithm will increase the functional reliability of the quadcopter ACS and the UAV as a whole by 1.17 times.

The increase of the quadcopter reliability reduces the number of its failures, which in turn allows it to save money through its multiple-use, reduce costs and time for its maintenance. It is planned that research results will be used in the development and making in the Aircraft Control Systems Department' quadcopter.

UDC 621.3

Chornomorets R., Chernyak M.

MEASUREMENT SIGNAL ERRORS OF UNMANNED AERIAL VEHICLE CONTROL SYSTEM ELEMENTS AND METHODS OF THEIR REDUCTION

Introduction. Currently, the problem of reducing noise in electrical equipment is important, because a noise in the system affects its components and can cause unpredictable behavior of the electrical system. This is especially important onboard of unmanned aerial vehicle (UAV), where all components are located close to each other and their noise has a significant cross-effect. Conductors passing through a noisy environment can pick up a noise and direct it to another circuits, where it creates interference. Some examples of such noise problems are: degraded accuracy characteristics of microcontroller modules (Analog-to-Digital Converters (ADC), Phase-Locked Loops (PLL) and other) due to noise on supply and reference voltages, wrong acquisition of the digital signals and interference with global navigation satellite system (GNSS) or remote-control system of UAV.

The research of the influence of electrical noise, which is formed by the components of the UAV control system (engines, electric motor controllers, microcontroller etc.), on the performance and noise protection of electronic components of the UAV control system was done.

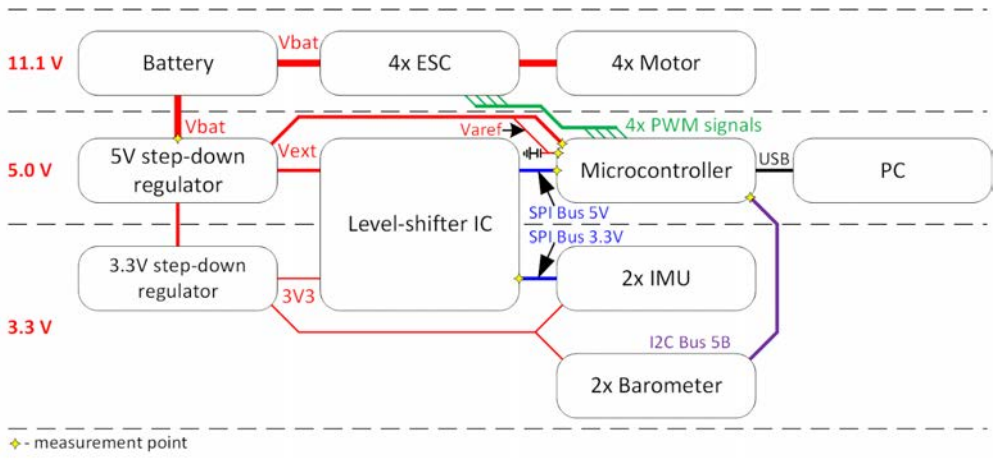

Fig.1. Structural scheme of the UAV

Scientific and technical results. In the experimental research of noise in the UAV control system were measured: battery voltage Vbat (~11.1V); input voltage of the microcontroller Vext (5V); input reference voltage of the microcontroller Varef (5V).

The main sources of noise and their amplitudes under different conditions were determined during the research. It was concluded that the main sources of

electrical noise in the UAV control system are: high currents, consumed by electronic speed controllers (with motors), high-speed toggling of clock signal of SPI / I2C communication, regulation by step-down voltage regulator and internal processes inside the microcontroller due to work of flight control firmware. The waveforms of generated noises, caused by each source were measured with oscilloscope and depicted in the main research paper.

Noise on battery voltage Vbat:

- Continuous operation of the engine creates oscillations at a frequency of 24 kHz with an amplitude of up to 1.07 Vpp.
- Motor startup causes an undershoot in battery voltage with fading oscillations with an amplitude of up to 2.45 Vpp.

Noise on power supply voltage Vext:

- Noise from the battery voltage Vbat has an insignificant effect on Vext due to its attenuation by the onboard step-down 5 V voltage regulator. Amplitude of fluctuations reaches up to 10 mVpp on Vext at oscillations on Vbat up to 2.45 Vpp.
- The noise from the clock signal of the SPI bus has the largest amplitude due to the fast driver of the output pins of the voltage level-shifter IC. The amplitude reaches 75 mVpp.
- The noise from the clock signal of the I2C bus can be significantly reduced by configuring the slower driver of the output pins of the microcontroller.
- The noise from the step-down regulator consists of oscillations at frequencies of 37 kHz and 416 kHz with amplitudes of 30 mVpp and 18 mVpp, respectively.

Conclusion. The minimum noise when the microcontroller is suspended is 38 mVpp. During the normal operation of the microcontroller as a flight controller, the noise increases to 43 mVpp.

UDC 629.7.015: 533.69.048.5

Hevko B., Bondar Y.

TURBULENCE LOADS ON THE WING OF THE TURBOJET AIRPLANE

Introduction. Flight in turbulent air is one of the main design cases for determining the strength under the influence of dynamic loads; especially this applies to the strength of the wing. The dynamic loads acting on the design of aircraft, is an extremely important problem for aviation. In the problems of durability two types of gusts of turbulent air are considered: discrete gust and continuous turbulence. Extreme single-gust loads are used to determine the static strength of the aircraft, while turbulence loads are also used to determine the structural life.

The aim of the study is to determine the discrepancy between the results of the calculations of loads from discrete gusts and continuous turbulence on the elastic wing of a regional turbojet airplane using: dipole lattice method (DLM), high order panel method (Panel), dipole lattice and constant pressure method (DLM/CPM) for mathematical modeling of aircraft flow.

According to the requirements of CS-25, gusts are considered that are normal to the flight path and uniform at spanwise. Random gusts at continuous turbulence are described by the spectral density (PSD) of gusts suggested by Karman.

Scientific and technical results. For the calculation of loads discrete gusts, the range of Design Gust Velocity, U_{ds} considered from 9.2 to 106.8 m (30 ÷ 350 ft). And for continuous turbulence, the scale of turbulence, L = 762 m (2500 ft).

The finite element model of the aircraft design is given by a multilevel tree, whose nodes are sub-structures. These substructures are presented in the form of elastic beams (ERB), which allow for all types of deformation. The elastic beam is used to model the fuselage, wing console, control surfaces, engines, pylons and tail unit. Each ERB is characterized by stiffness and mass distributions.

Aerodynamic surfaces are modeled as follows:

Fuselage – Body wrapping;

Wing, control surfaces, fin, stabilizer – Wing surface;

Engines – Orthogonal flat surface.

Tones and shapes of self-oscillations of a aircraft structure are determined on the basis of partial tones of substructures by means of the modal synthesis algorithm used in IMAD. To ensure the required accuracy of modal structural analysis, 25 first tones of symmetric and antisymmetric vibrations were calculated. In addition to, the design model of the aircraft was refined based on Ground Vibration Testing (GVT) data.

The calculations were performed for the model of regional turbojet airplane, such as AN-148 or similar, with a mass of 36.4 t, with a wing area of 28.7 m^2, when flying at a speed of Vc_{cas} = 530 m/c, at an altitude of 10000 m (M_c = 0.8). For calculating loads flows around the aircraft were considered quasi-stationary or non-stationary.

The results were analyzed by comparing the obtained values of the transverse force Q_y and the bending moment M_x, and their distribution by the wingspan. The maximum values of loads from discrete gusts were obtained at the range U_{ds} = 60 ÷ 70 m. In the wing root sections, the smallest difference between the obtained values of the loads is observed, and when approaching the endings, this difference significantly increases in relative values.

However, in the root section of the wing for the DLM, the transverse force Q_y values at horizontal flight are 23 – 25% lower than for other methods. VFM failed to obtain loads from discrete gust and continuous turbulence at horizontal flight, as for this method the efficiency of the rudder proved to be insufficient to balance the model of aircraft.

The calculations with non-stationary flow showed an increase in the loads on the aircraft structure, up to 3% in the root sections of the wing and more than 20% in the end sections, when compared with quasi-stationary flow.

For continuous turbulence these differences are more significant than for discrete gusts. The biggest difference of loads is when using DLM, and the smallest is in the Panel method.

The magnitude of the root-mean-square (RMS) value of load increment from turbulence is almost the same for all the considered methods. The main and significant difference between the methods used is manifested in the calculation of loads in horizontal balanced flight, where the use of DLM/CPM allows obtaining the lowest values of loads. In any case, the total loads are smaller when using the Panel method, but this difference varies within 0.1 ÷ 2%

Conclusion. Choosing the best analytical and computational methods for determining the loads on the aircraft will allow you to design the optimal aircraft design and provide the necessary flight safety. It will also reduce the time of design and research work in the future.

UDC 629.735.7

Hryshchenko D.S., Ponomarenko S.O.

NON-INVARIENT APPROACH TO THE SYNTHESIS OF ALGORITHMS OF INTEGRATED INERTIAL-SATELLITE NAVIGATION SYSTEMS OF UNMANNED AIRCRAFT

Introduction. Integrated inertial-satellite navigation systems (INS + SNS) are widely used in the control systems of modern unmanned aerial vehicles (UAVs). They are a combination of two independent systems - inertial navigation system (INS) and satellite navigation system (SNS). Hardware and algorithmic integration of these navigation systems, operating on different physical principles, allows you to combine the advantages and compensate for the disadvantages inherent in each of the systems separately.

In previous studies [3], the evaluation of navigation parameters and corrections to the readings of sensors in the procedure of nonlinear discrete filtering occurs together with the adjustment and extrapolation of the corresponding covariance matrix of error estimates. And this is implemented in one filter of Kalman type of large dimension, leading to instability of computational procedures. And there is a need to increase the reliability of calculations.

To synthesize algorithms of the integrated INS + SNS of the UAV navigation complex on the basis of the noninvariant approach with the increased computational reliability due to carrying out a problem of calculation of corrections to indications of inertial sensors in separate computing procedure.

Scientific and technical results. Synthesis of algorithms of integrated inertial-satellite systems. The algorithm of the noninvariant compensation scheme of complexing of inertial sensors of the primary information and onboard correctors of the SNS with the increased computational reliability is offered in the work. In the proposed algorithm, the navigation vector of the nonlinear filter includes only navigation parameters (components of travel speed, coordinates, orientation parameters). The procedure of nonlinear discrete filtering in the proposed version implements the operation of refining estimates of navigation parameters and the corresponding covariance matrix of estimates taking into account current information from navigation correctors and the operation of extrapolation of estimates of navigation parameters and covariance matrix of errors using current readings.

To estimate the parameters of models of systematic errors of inertial sensors at a given initial time interval $[t_0, t_0 + T]$ using information from navigation correctors, a special linear regression procedure is proposed, based on the methodology of sensitivity theory [6].

The proposed version of the non-invariant compensation scheme of complexation involves the implementation of the following stages:

Stage 1. Clarification of estimates of the vector-column of navigation parameters and the covariance matrix of errors of estimates at the starting point of inclusion of navigation correctors $t = t_0$. This operation is implemented using known procedures [1]:

$$\hat{\tilde{X}}(t_0) = \tilde{\bar{X}}(t_0) + K_0\{\bar{Y}(t_0) - h[\tilde{\bar{X}}(t_0), t_0]\}; \quad (1)$$

$$\hat{P}(t_0) = [E - K_0 H_0]P_0;$$

where $K_0 = P_0 H_0^T (H_0 P_0 H_0^T + R_0)^{-1}$;

$$H_0 = \frac{\partial h[\bar{X}(t_0), t_0]}{\partial \bar{X}};$$

P_0 - the initial value of the covariance matrix of estimation errors;

R_0 - covariance matrix corresponding to the error vector $\bar{\eta}(t_0)$.

Stage 2. This step is implemented at a given initial time interval $[t_0, t_0 + T]$ and involves the operation of the procedure of nonlinear discrete filtering only in the mode of extrapolation of estimates of navigation parameters and the covariance matrix P (without correction of these estimates). Formally, the relevant operations can be represented as:

$$\hat{\tilde{X}}(t_{i+1}) = \hat{\tilde{X}}(t_i) + f[\hat{\tilde{X}}(t_i), \tilde{\bar{Z}}(t_i), t_i]\Delta t; \quad (2)$$

$$P(t_{i+1}) = \Phi(t_i)P(t_i)\Phi^T(t_i) + Q(t_i); \quad (3)$$

where $\Phi(t_i) = E + \frac{\partial f[\bar{X}(t_i), t_i]}{\partial \bar{X}}\Delta t$;

$Q(t_i)$ - covariance matrix corresponding to the vector of random perturbations $\bar{\xi}(t)$.

To construct a linear regression procedure for identifying the parameters of the models of systematic errors of inertial sensors, a matrix of sensitivity functions $U(t_i) = \frac{\partial \tilde{\bar{X}}(t_i)}{\partial \bar{\mu}}$ is used, which is calculated by integrating the following equation:

$$\dot{U}(t) = \frac{\partial f\{\hat{\tilde{X}}(t), \bar{Z}(t) + \chi[\bar{\mu}, \tilde{\bar{Z}}], t\}}{\partial \hat{\tilde{X}}} U(t) + \frac{\partial f\{\hat{\tilde{X}}(t), \bar{Z}(t) + \chi[\bar{\mu}, \tilde{\bar{Z}}], t\}}{\partial \bar{\mu}}, \; U(t_0) = 0. \quad (4)$$

The value of the matrix $U(t_i)$ for discrete moments of time $t_i = t_0 + j\Delta T$, $j = 1, 2, \ldots, N$, is used to construct linear regression functions of this kind

$$G_\Sigma \bar{\mu} = \Delta \bar{Y}_\Sigma \quad (5)$$

where

$$G_\Sigma = (G_1^T, G_2^T, \ldots, G_N^T)^T; \; \Delta \bar{Y}_\Sigma = (\Delta \bar{Y}_1^T, \Delta \bar{Y}_2^T, \ldots, \Delta \bar{Y}_N^T)^T;$$

$$G_j = \frac{\partial h[\hat{\tilde{X}}(t_j), t_j]}{\partial \bar{X}(t_j)} U(t_j); \; \Delta \bar{Y}_j = h[\tilde{\bar{X}}(t_j), t_j] - \bar{Y}(t_j);$$

$$j = 1, 2, \ldots, N.$$

The operation of identifying the parameter vector $\bar{\mu}$ for the regression model (5) is represented as follows:

$$\hat{\bar{\mu}} = G_{\Sigma}^{\oplus} \Delta \bar{Y}_{\Sigma}, \tag{6}$$

where $\oplus$ – symbol of the operation of pseudo-rotation of the matrix G_{Σ} by the Greville method [1].

Stage 3. When the procedure of nonlinear discrete filtering implements both the operation of refining the estimates of the covariance error matrix $\hat{P}(t_i)$ and the vector of navigation parameters $\hat{\bar{X}}(t_i)$ from the information from the navigation correctors $\bar{Y}(t_i)$, and the operation of extrapolating the estimates of the matrix $\hat{P}(t_i)$ and the vector of navigation parameters $\hat{\bar{X}}(t_i)$ using current readings of inertial sensors.

$$\Delta \bar{Z}_{\Pi}(t_i) = -\chi[\hat{\bar{\mu}}, \tilde{\bar{Z}}(t_i)]. \tag{7}$$

In a special case, when only the offset readings are taken into account in the sensor error models

$$\Delta \bar{Z}_{\Pi} = -\Delta \hat{\bar{Z}}, \tag{8}$$

where $\Delta \hat{\bar{Z}} = \left(\Delta \hat{a}_{x1}, \Delta \hat{a}_{y1}, \Delta \hat{a}_{z1}, \Delta \hat{\omega}_{x1}, \Delta \hat{\omega}_{y1}, \Delta \hat{\omega}_{z1}\right)^T$ - vector of estimates of the displacement of the readings of inertial sensors in the bound basis $OX_1Y_1Z_1$.

On the known results of the theory of sensitivity [6] we can show that the condition for solving the problem of linear regression (observability of the components of the vector $\bar{\mu}$) is the nondegeneracy of the Gram matrix:

$$\Gamma = \int_{t_0}^{t_0+T} U^T(\tau) U(\tau) d\tau, \tag{9}$$

based on sensitivity vector functions, in other words the linear independence of sensitivity vector functions on the observation interval $[t_0, t_0 + T]$.

Conclusions. The simulation results confirm the efficiency of the proposed algorithm of non-invariant compensation scheme of complexing of inertial sensors and onboard navigation correctors of SNA UAVs. The dimension of the state vector of the integrated INS + SNA navigation system can be reduced in comparison with the known integration algorithm by the number of parameters of inertial sensors (3-zero offset accelerometers and 3-reduced drifts of gyroscopes), which increases the computational reliability of the proposed algorithm.

References:

1. Sineglazov V.M, Zakharin F.M.// Theoretical bases of designing integrated navigation systems of unmanned aerial vehicles. - Kiev: Education of Ukraine. 2015. - 340 p.

2. Stepanov O.A.// Peculiarities of construction and prospects of development of inertial-satellite navigation systems // Integrated inertial-satellite navigation systems. - St. Petersburg: Central Research Institute of Electrical Equipment. - 2004. - P. 25-43.

3. Zakharin F.M, Ponomarenko S.A .//Principles of navigation system design of UAV // Electronics and control systems. №3 (45), 2016. Kyiv. NAU. P.103-108.

4. F.M Zakharin, V.M Sineglazov, M.K Filyashkin.//Algorithmic support of inertial-satellite navigation systems: monograph /; Nat. aviation. un-t. - K., 2011. - 319 p. - Bibliogr .: 34 titles - ukp.

5. Pronkin A.N, Kuznetsov I.M, Veremeenko K.K Integrated.// UAV navigation system: structure and study of characteristics

6. N.E Khatsko, //Modern mathematical models of error compensation of inertial sensors for use in calibration experiments

7. A.V. Proletarskiy, K.A.// Neusypin methods of correction of navigation systems and aircraft complexes

8. Babich O.// Information processing in navigation systems. - M .: Mashinostroenie, 1991.

UDC 629.783

Ivanko T., Ryzhkov L.

SYNTHESIS AND ANALYSIS OF INTEGRATED ACCELEROMETER/GPS SYSTEM FOR OPERATION IN GPS SIGNAL LOSS CONDITIONS

Introduction. Modern inertial-satellite navigation systems (ISNS) are integrated by a certain data filtering algorithm. The development of these algorithms from the extended Kalman filter [1-2] to complementary filters (CF) of Madgwick [3], Mahony [4], as well as a number of information processing algorithms based on the combination of Kalman filter and complementary filter [5-6] don't provide an effective solution in case of loss of GPS signal.

It is well known that the satellite navigation system provides the correct motion parameters when receiving signals from 4 or more satellites. This condition may not be met in the presence of obstacles to data receiving - high building density, tunnels, mountains, active obstacles, etc. [7].

To date, the following methods have been proposed to solve this navigation problem: designing a tightly coupled inertial-satellite navigation system [8-9] and using cooperative localization in UAV group flight [10]. But these methods have their drawbacks: for the first it is the need to develop a receiver, the operation of the system in the presence of a signal from at least one satellite; for the second - restriction of use only for the UAV group.

In this way, the task of developing a scheme of data integration for the accelerometer and GPS-receiver for operation in gps signal loss conditions is relevant. It is expedient to use a complementary filter to preserve the useful signal and reduce sensor interference.

Scientific and technical results. Integration of accelerometer and GPS-receiver. There are two modes for efficient operation of the system: the mode of autonomous operation - stand-alone mode - in case of loss of GPS-signal and the mode of complementary filter in its presence. Let the switch be the control signal u, which is fed to the units responsible for the autonomous operation of the system.

The object of observation has navigation parameters: coordinate, speed and acceleration. They are input values for sensors (Fig. 1). The measured value of displacement x_{GPS} and acceleration a_{AC} is fed to the input of the complementary filter, the structure of which is described by equation 1. In the case of correct operation of the GPS receiver, the output signal of the complementary filter is transmitted to the relay and is the output signal of the system.

$$W_1(s) = \frac{s^2}{s^2 + s + 1}; W_2(s) = \frac{s + 1}{s^2 + s + 1}. \quad (1)$$

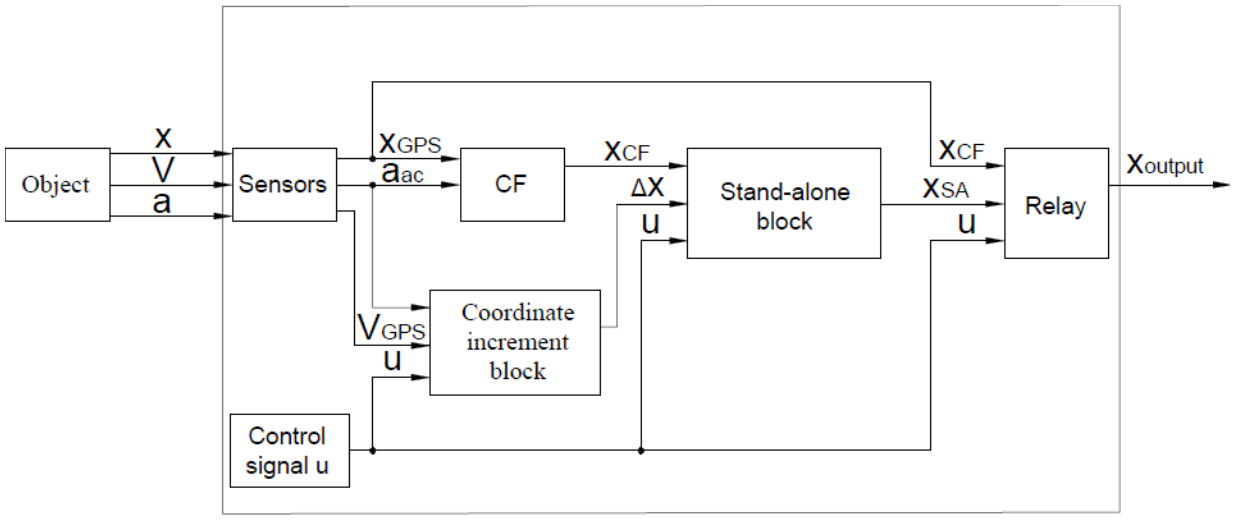

Fig. 1. Block diagram of integrated accelerometer/GPS-receiver system

Fig. 1 shows: x, V, a - object motion parameters, x_{GPS} - measured value of displacement x, a_{AC} - measured value of true acceleration $\ddot{x}$, u - control signal, x_{CF} - displacement at the output of the complementary filter, V_{GPS} - measured value of velocity, Δx is the increment of the coordinate, x_{SA} is the displacement at the output of the stand-alone block, x_{output} is the output value of the measured value.

In stand-alone mode, the current V_{GPS} value is tracked and stored in the coordinate increment block, the input signals of which are also the accelerometer data and the control signal. In case of GPS signal loss condition the acceleration is twice integrated. The result of integration of speed V_{GPS} is add to the received value that in the sum gives increase of a coordinate Δx. This coordinate increment is the addition to the coordinate from the complementary filter, which is stored in the stand-alone block. The output signal of the stand-alone block is fed to the relay and is the output signal of the system in case of loss of GPS signal.

Modeling of the integrated system. The work of schem, which is presented in Fig. 1, is investigated by simulation modeling in the MATLAB-Simulink environment. Input simulation parameters: a = 0.01 m / c2, δ / g = 1.75 * 10-3, harmonic error of GPS receiver δx = 1sin20πt m, simulation time is t = 250 s.

The otkl-podkl unit generates a control signal to simulate the loss of a GPS signal. Control signal 0 corresponds to the connected GPS mode, 1 - disconnected.

The result of testing the integrated accelerometer / GPS-receiver system displays a comparing the errors of the complementary filter ΔX_{CF} and integrated system $\Delta X_{COMPLEX}$ in the condition of loss GPS signal. The accumulation of error corresponds to periods of absence of satellite signal. Output simulation

parameters: time of absence of satellite system's signal t_1 = 20 s, $\Delta X_{COMPLEX}$ = 3,44 m, ΔX_{CF} = 7,98 m; t_2 = 30 s, $\Delta X_{COMPLEX}$ = 7,30 m, ΔX_{CF} = 34,49 m.

Conclusion. The integrated system consisting of an accelerometer and a GPS receiver has been created, designed to operate in the condition of a short-term loss of the GPS signal. The structure of the system, which includes the complementary filter, for the decision of a navigation problem in the conditions of loss of a GPS signal is offered. In the absence of a satellite signal, the error of the synthesized system is directly proportional to time and is less than the error of the system with complementary filtering on the order for time t = 30 c. This area of research is promising, as it will allow the use of more accurate navigation systems in conditions of natural and man-made obtacle.

UDC 629.735.33

Kalapun N., Bondarenko O.

LOCAL PASSENGER TRAFFIC COMPLEX BY MEANS OF LIGHT AIRCRAFT

Introduction. The aim of the study choose an infrastructure development option and an aircraft for local air travel. To achieve this goal we solve the following problem: the typical infrastructures of such countries as Canada, the USA (especially Alaska) were analyzed. Canadian airspace was chosen as the basic structure, with the exception of routes of international importance. It consists of small aerodrome structures of the type of base and regional aerodromes with refuelling capabilities, specified lengths and landing surfaces. We chose a system of base and regional airfields for Ukraine based on economic opportunities, features of the steppe part of the country (geographical conditions), as well as the availability of airfields that are subject to international designation as base and are not used for their intended purpose in recent years.

Routes for flights and construction of a network of aerodromes were taken from the conditions of providing a comfortable and fast flight between points, where this was not possible due to the unspecified condition of roads for other land transport (Fig. 1).

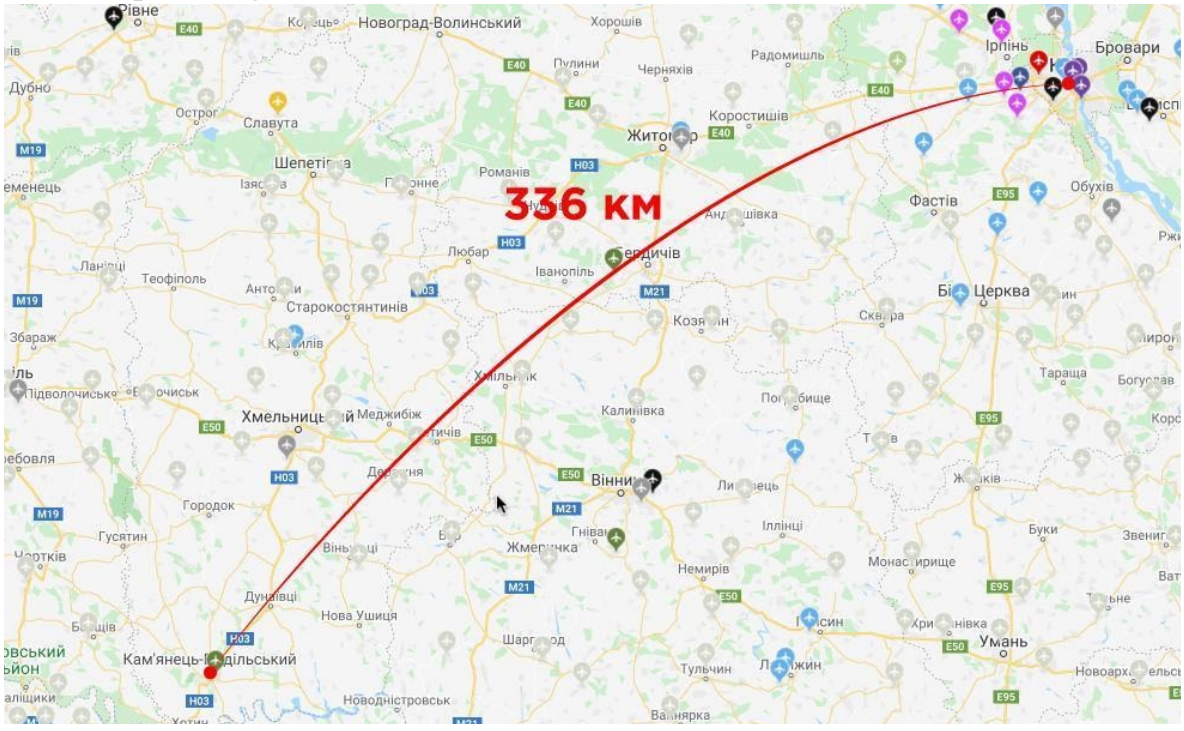

Fig. 1 - Map of the selected route Kyiv - Kamianets-Podilskyi

Scientific and technical results. Among the airfields, a base with columns for refueling and service personnel was chosen. 4 types of aircraft for use in the following air transportation were analyzed:

- four-seater Cessna-172 from composite materials which needs to be serviced in the conditions of special technologies;
- multi-seat domestic aircraft of basic duralumin configuration (An-3, An-28), which require a separate repair site at existing airfields;
- five-seater LA-50 (Patriot), which also requires regular inspection with possible replacement of parts.

The range and duration of flights were calculated.

$$L = \frac{G_{т.р}}{q_k} = \frac{G_{т.р} 3{,}6 V_H}{q_ч} = \frac{G_{т.р} 3{,}6 V_H}{c_e N_e} = \frac{G_{т.р} 3{,}6 V_H 75 \eta_B}{c_e P V_H}$$

where L - distance, $G_{т.р.}$ - total fuel mass, q_k - the number of kilometers of fuel consumption, $q_ч$ - hourly fuel consumption, $V_н$ - cruising speed, c_e - specific fuel consumption, N_e - power, P - thrust, $\eta\,\eta_B$ - efficiency.

$$T = 75 \frac{G_{т.р}}{G_{ср}} \frac{K}{V_H} \frac{\eta_B}{c_e}$$

where $G_{ср.}$ is the normal mass of the aircraft, K is the quality factor. Fuel consumption was taken from the technical documentation of aircraft. The results of the analysis are systematized in table 1.

Table 1. Results of the analysis

	AN-3	Cessna	AN-28	LA-50	
Quantity	10,00	3,00	17,00	4,00	passengers
Distance	336,00	336,00	336,00	336,00	km
Charge for fuel	28,50	28,50	28,50	28,50	uah/litres
Service	1000,00	500,00	2000,00	700,00	uah/flight
Payments for assistance and pilots	2300,00	1300,00	6300,00	1300,00	uah/flight
Time	1,46	1,47	1,00	1,20	hours
Fuel	554,62	55,74	405,89	28,45	litres
Price of fuel	15806,62	1588,47	11567,81	810,77	uah
Payments for the service possibilities	225	1150	4000	1700	uah
Fees for 1 flight	21242,28	4877,32	25854,59	4791,84	uah
Price for 1 ticket	2124,23	1625,77	1520,86	1197,96	uah

The main feature was the cost of transporting one passenger. A number of factors are taken into account, including depreciation for aircraft repairs, approximately 0.1% of the cost of aircraft.

An-3 - was the most expensive in terms of fuel.

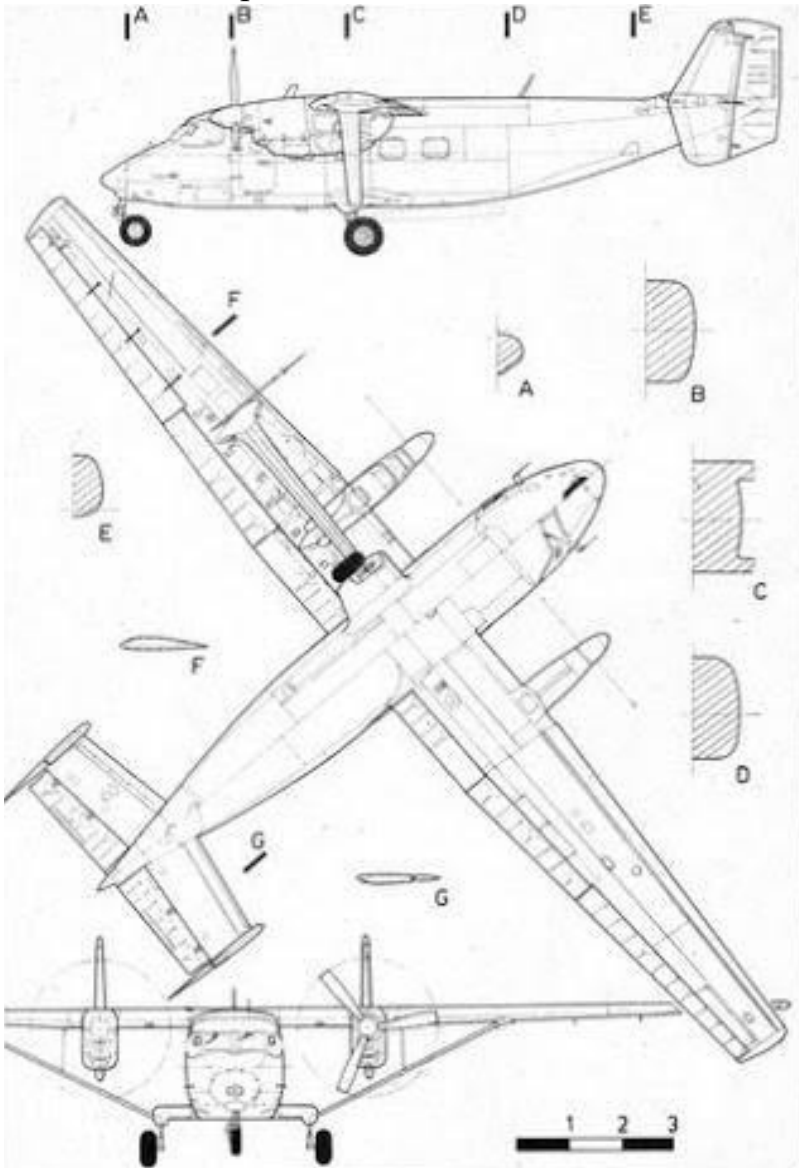

Fig. 2 - Scheme An-28

Conclusion. A combination of two equivalent transportation options is suitable for certain tasks on the route with a distance of 336 km and passenger capacity, depending on the demand for transportation, which can operate in parallel:

- An-28, which requires a runway of 600-800 m, which meets the conditions of this regional airfield, and regularly recruits the required number of passengers;
- small aircraft type LA-50.

UDC 533.694.24

Komarov B., Zinchenko D.

ADAPTIVE FAN WING MECHANIZATION

Introduction. Airplane flight speed in cruise mode, one of the most important parameters. But during takeoff and landing, a high takeoff speed is not needed. It is better, on the contrary, to lower it as much as possible to reduce the required distance of the runway and to increase safety. The way out of this situation is takeoff and landing mechanization. In previous works, the optimal aerodynamic cruising flight profile for the fan wing system was created, but it also does not allow obtaining the necessary advantage during takeoff and landing. Therefore, on the trailing edge of the wing, it was necessary to create flaps, which simultaneously the role of a reversing system in the spoiler mode, and when flying with small differential deviations, in the ailerons mode.

The main goal of the work is to determine the influence of adaptive wing mechanization on aerodynamic characteristics.

The study was conducted based on simplified models and models created using 3D printing. To determine the aerodynamic characteristics, modelling was performed on the basis of a class of methods for computational aero-hydrodynamics of particles and Boltzmann lattice equations. The technology used allows to model complex processes of CFD with frequent transitions between states, the real movement of geometries, complex multiphase flows, free-surface flows and interaction between liquids and structures.

Scientific and technical results. The wing was first tested in a take-off configuration with the flaperon released (Fig. 1.). From previous experiments, this position allows changing the angle of the thrust vector by 10 degrees relative to the cruising configuration.

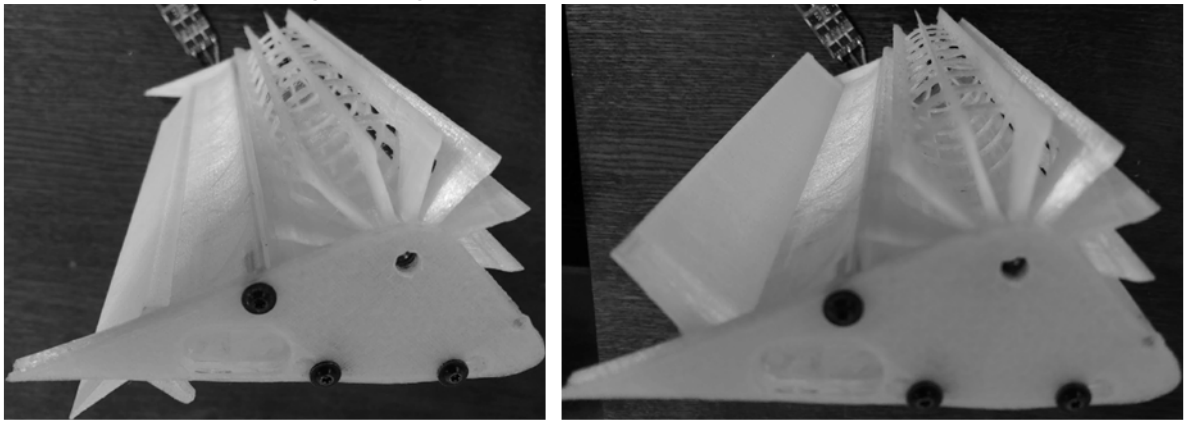

Fig. 1. Flap and reversive spoiler configuration

This reduces lift-off speed while increasing C_D by 8%, and at the same time increases the lift force, which will affect the take-off length of the fan wing system. In the landing configuration with a lower rotational speed of the

cross-flow fan, with the same deviation of the flap, the angle of the thrust vector can vary up to 12 degrees. This allows to reduce V_{App} by more than 20% even compared to traditional wings with significant mechanization. After plane touchdown, adaptive flap at spoiler mode generates against direction thrust from the adaptive fan wing, 40-50% of it reversible. The rest of the thrust is directed in the direction of the lifting force, which will create a significant clamping force and will not allow the plane to break away from the ground during the run with the transfer of the flap mode to the spoiler mode.

The use of an adaptive system as ailerons is also advantageous, due to the significant blowing of the surfaces, with a simultaneous change in the thrust vector on the wing consoles, even with minor deviations, there are significant changes in the orientation of the aircraft. Due to which ailerons can be installed not even on the root sections of the wing and they will have more than sufficient efficiency. At the same time, use a differential change in speed when using at least one section with a fan wing propulsion on the wing console to reserve controls.

Conclusion. Adaptive mechanization, at least flaperon, with the switch to spoiler mode can increase the takeoff and landing characteristics of the fan wing plane. Experimental calculations and tests have shown that changing the thrust vector and increasing the lift force will reduce the V_{lof} speed by more than 10% compared to an aircraft that uses a non-adaptive rotor wing. However, the use of an adaptive wing will reduce V_{App} by 15%. Also in spoiler mode, after touchdown, the reverse mode will reduce the range to stop with adaptive wing, and will increase safety. Using the fan wing adaptive system simultaneously as ailerons twice is good for backup. Due to the simplicity of construction and the small number of moving parts, the system is very reliable. The increase in wing mass is insignificant about 5%. For further experiments, a flying model demonstrator will be created using the proposed wing.

UDC 629.7.05

Kovalov A., Nechyporenko O.

IMPROVING THE ACCURACY AND RELIABILITY OF MULTICOPTER MAGNETOMETRIC SYSTEM

Introduction. As a result of the development of electronics and technology of microelectronic mechanical systems, MEMS magnetometers appeared, which provide the function of a compass in a chip design and are part of the orientation system of multicopters. The relevance of the use of MEMS-magnetometers on board multicopters is due to their low weight and size, simplicity of design and cheapness of the device.

The aim of this work is to find a method to increase the accuracy and reliability of the magnetometric system of the multicopter to improve the characteristics of the orientation system, which includes a magnetometer, which will increase the reliability of the multicopter as a whole and ensure its reliability during flight. This is due to the low accuracy and reliability of MEMS magnetometers.

Scientific and technical results. During the design of the magnetometric system, a number of factors were identified that affect the measurement result of the magnetometric system, thereby distorting it, namely: vortex interference, soft and hard iron, located nearby. To eliminate such problems, the method of mathematical compensation was performed. A constructive method was used to eliminate vortex interference caused by non-constant currents in the conductors near the magnetometric system.

To increase the accuracy and reliability of the magnetometric system of the multicopter, a method of complexing three separate magnetometers into one system, installed parallel to each other, the axes of sensitivity of which are directed in one direction, was developed. This reduced the effect of the error associated with the non-perpendicularity of the sensor axes. Also, the presence of several sensors connected in parallel is the application of the method of loaded redundancy, which significantly increases the reliability of the magnetometric system as a whole.

The developed processing method implements the following processing algorithm: 1) the measurement results of three separate magnetometers are averaged, which gives a more accurate measurement result; 2) the method of detection of gross errors and emissions (parametric failures of sensors) and their exclusion from measurement results, and also detection of zero output signals of magnetometers (functional failures of sensors) is added. That is, if one of the three magnetometers will show an orientation angle far from the readings of the other two, or will be missing its output signal, its response will not be taken into account in the subsequent calculation of the angle of rotation.

A computational program for processing the output signals of magnetometers has been developed, the installation of which on the Arduino

microcontroller allowed to directly calculate and test the orientation of the aircraft in space, which ensures its trouble-free flight.

Practical implementation. The results of the study will be further applied on board the multicopter. Improving the accuracy and reliability of the magnetometric system reduces the probability of failure of the multicopter orientation system.

UDC 681.518.3

Kushniruk M., Nechyporenko O.

IMPROVING THE RELIABILITY OF QUADCOPTER AUTOMATIC LANDING COMPLEX SYSTEM BASED ON A BAROMETRIC ALTIMETER AND ULTRASONIC RANGEFINDER

Introduction. Research actuality is caused by the requirements to increase the reliability of the quadcopter automatic landing system.

Research purpose is to improve the reliability of the complex (integrated) automatic landing system of quadcopter, which will land the quadcopter without fail when the control signal is send.

To achieve this purpose, it is proposed to increase the reliability of the automatic landing system by adding to the automatic landing system (ALS) a quadcopter altitude measurement system (AMS), which combines functional and structural load redundancy, i.e. combined one ultrasonic rangefinder (UR) with two micromechanical barometric altimeters (MBA).

Scientific and technical results. To increase the reliability of the ALS, a new integrated AMS has been developed, which uses three measuring devises: two MBAs based on a piezoresistive pressure sensor and one UR. In terms of reliability, it is a combination of functional redundancy (combination of MBA and UR, which have the same functional purpose, but use different physical principles of measurement) and structural redundancy (parallel combination of two identical sensors - two identical MBAs).

Experimental studies of the working condition (up state) of the operating model of AMS were carried out, in which used the following means of measuring the flight altitude of the quadcopter: two barometric altimeters, developed on the basis of digital piezoresistive atmospheric pressure sensor (module with barometer, type BMP-280, company BOSCH), and ultrasonic range-finder, type HC-SR04, which has no "blind spots" and can measure a distance of 0 to 1.5 m. The noise of the two MBVs is smoothed using a simplified Kalman filter.

The analysis of the test results of the AMS operating model showed the efficiency of the developed system. The developed algorithm for flight altitude measuring is occupied by little space in the memory of the processor which will allow to install it in even the simplest microcontrollers.

Practical application. The complex ALS of the increased reliability is developed for use on board the quadcopter. It increases the reliability of the quadcopter by 1.2 times, simplifies its operation, and allows to control the landing of the quadcopter, even an inexperienced person.

UDC 681.518.3

Nekrutenko V., Serdyuk.A.

INFLUENCE OF TRANSLATIONAL ACCELERATION ON THE MICROMECHANICAL GYROSCOPE OUTPUT SIGNAL ERROR

Introduction. Currently, the widespread use of micromechanical gyroscopes (MMG) in various equipment of public and military equipment.

The aim is to provide schematic solutions that will reduce the impact of interference created by the translational acceleration of the object. To analyze the possibilities of reducing the influence of translational accelerations on the measurement error of MMG of different structures. To improve the stabilization of the UAV in the air. Investigate the dynamics of micromechanical gyroscopes of different kinematic schemes, identify the dependences that determine the influence of rotation of the base on the motion characteristics of sensitive elements, in order to develop recommendations for calculation, design and improvement of gyroscopes.

The development of a gyroscopic device of a given accuracy requires a detailed study of the errors that are present in the output signal of the sensor. Such a study will develop methods to eliminate errors and improve the accuracy of the device. Consider the main sources of errors of the vibrating gyroscope with an additional frame, as well as methods for assessing and eliminating these errors.

Scientific and technical results. Investigate the motion of a sensitive element of a micromechanical vibrating gyroscope with an intermediate frame on the base, which performs angular motion at a constant speed $= \{0, 0, \}$ and translational with constant acceleration $\bar{w} = \{w_1, w_2, 0\}$.

The equations of motion of the sensing element in this case have the form:

1.1

$$\begin{cases} \ddot{x}_1 + 2h_1\dot{x}_1 + \left(k_1^2 - \Omega^2\right)x_1 - 2\Omega\dot{x}_2 = -w_1, \\ \ddot{x}_2 + 2h_2\dot{x}_2 + \left(k_2^2 - \Omega^2\right)x_2 + 2d\Omega\dot{x}_1 = q_2 - w_2. \end{cases}$$

The system of equations (1.1) is linear, and therefore, to find the solution of the system that corresponds to the reaction of the sensing element to a constant translational acceleration, we can use the principle of superposition. Take into account that the sensing element is affected by both translational acceleration and the forces of harmonic excitation. Then the effect of constant acceleration on the motion of the sensing element will be described by a particular solution of the system.

1.2

$$\begin{cases} \ddot{x}_1 + 2h_1\dot{x}_1 + \left(k_1^2 - \Omega^2\right)x_1 - 2\Omega\dot{x}_2 = -w_1, \\ \ddot{x}_2 + 2h_2\dot{x}_2 + \left(k_2^2 - \Omega^2\right)x_2 + 2d\Omega\dot{x}_1 = -w_2. \end{cases}$$

1.3

$$x_j = x_{j0} = const\,, \quad j = 1,2\,.$$

Substituting the solution (1.3) into the system (1.2) we obtain the following formulas for the shifts of the inertial mass and the frame from the constant acceleration:

1.4

$$x_{j0} = -\frac{w_j}{k_j^2 - \Omega^2} \approx -\frac{w_j}{k_j^2}\,, \quad j = 1,2\,.$$

As follows from formula (1.4), the reaction of the sensing element to a constant translational x acceleration will be a constant shift in the direction opposite to the direction of the acceleration vector and proportional to the magnitude of this acceleration. The constant component in the output oscillations of the inertial mass is eliminated by filtering the signal from the displacement sensor at the operating frequency. The greatest influence on the error of MMG when measuring the angular velocity Ω_y will provide a linear vibration in the YZ plane. Moment , due to the non-uniform stiffness of the suspension and the inertial forces acting on the rotor due to vibration acceleration W, acts in the same way as the gyroscopic moment r = Ω around the output axis OX.

1.5

$$M_x^H = F_z y - F_y z,$$

$$F_y = -mW_y; \qquad F_z = -mW_z; \qquad y = \frac{mW_y}{G_y}; \quad z = \frac{mW_z}{G_z};$$

m – rotor mass; W_y, W_z – vibration acceleration in the direction of the respective axes; G_y, G_z – the stiffness of the elastic suspension in the direction of the respective axes.

We give equation (1.5) as follows:

1.6

$$M_x^H = -m^2 W_y W_z \left(\frac{1}{G_y} - \frac{1}{G_z}\right) = -mW_y W_z \left(\frac{1}{\omega_{y0}^2} - \frac{1}{\omega_{z0}^2}\right) =$$

$$= \frac{mW_y W_z}{\omega_{z0}^2}\left(1 - \frac{\omega_{z0}^2}{\omega_{y0}^2}\right),$$

0, 0 – the frequency of natural oscillations of MMG in the direction of the respective axes. We add to the consideration of the coefficient of non-uniform stiffness of the suspension:

1.7

$$K_{yz}^H = 1 - \omega_{z0}/\omega_{y0}$$

and rewrite expression (1.6) in the form:

1.8

$$M_x^H = \left(K_{yz}^H m W_y W_z\right)/\omega_{z0}^2.$$

When the equality 0 = 0 (suspension is rigid) = 0.

Assume that the components of vibration acceleration have the same frequencies ωv, but shifted in the phase of influence ψ:

$$= {}_0 \sin {}_{\text{в}} ; \quad = {}_0 \sin({}_{\text{в}} +),$$

де $_0$ = = – amplitude of vibration acceleration.

We bring to the following kind:

1.9

$$W_y W_z = W_0^2 \left[(1 - \cos^2\omega_{\text{в}}) \cos\psi + \frac{1}{2}\sin(2\omega_{\text{в}} t) \sin\psi\right],$$

In order to minimize the impact of non-uniformity, it is necessary to observe the following inequalities:

1.10

$$M_{\text{г}} = H_0\Omega_y \gg \left(K_{yz}^H m W_0^2\right)/\omega_{z0}^2,$$

hence we obtain a restriction on the coefficient of non-uniform stiffness:

1.11

$$K_{yz}^H \leq \frac{H_0\Omega_y\omega_{z0}^2}{mW_0^2}.$$

From the formula (1.11) we can conclude that the coefficient of non-uniform stiffness is greater the higher the frequency 0, but due to the small thickness of the rotor compared to its diameter it is difficult to obtain a high value 0, because the rotor is deformed by large vibrational perturbations.

From expression (1.10) a restriction on the maximum value of the vibration amplitude can be obtained:

1.12

$$W_0 \leq \omega_{z0}\sqrt{\frac{H_0\Omega_y}{K_{yz}^H m}}.$$

For real MMG parameters, the difference in $_{yz}$ frequencies 0 and 0 is significant and the value of the coefficient of non-uniform stiffness approaches one, as a result of which the influence of linear vibration on MMG errors is amplified. Linear vibration at the coefficient of non-uniform stiffness → 1 can lead to significant distortions of secondary (initial) oscillations of MMG. It should be borne in mind that the perturbing moment has a frequency of secondary oscillations and therefore it cannot be eliminated by filtering the output signal MMG.

At в <0,5 0 the resonant amplification of the perturbing moment due to the non-uniform stiffness of the suspension is absent, ie the requirement for

uniform stiffness of the suspension is eliminated. Obviously, in this case the conclusion about influence of its unequal rigidity should be made on the basis of equality:

1.13

$$M_x^H = H_0 \Omega_y \Omega_x,$$

- determined by the formula (1.8).

To reduce the effect of linear vibration on the output signal of MMG it is necessary:

- reduce the coefficient of non-uniform stiffness of the suspension in a plane that is perpendicular to the axis of the secondary (output) oscillations of the rotor;
- increase the frequency of natural oscillations of the rotor (you can use filtering methods to select a useful signal);
- control the frequency of vibrational perturbations, which should be less than half the frequency of the natural oscillations of MMG relative to the output axis.

Conclusion. During the work the following theoretical and practical results were obtained:

1. The influence of linear vibration of the base on MMG with non-uniformly rigid suspension is estimated. Restrictions on the maximum vibration amplitude 0 and the coefficient of non-uniform stiffness are obtained
2. The traditional measures to reduce the effect of linear vibration on the output signal of MMG are identified.

UDC 629.783

Prymushko A., Ryzhkov L.

SYSTEM FOR DETERMINING OF THE ORIENTATION OF MOVING BODIES BASED ON COMPLEX SYSTEMS OF DISCRETE TYPE

Introduction. In [1] it was proved that a complementary filter can have the same accuracy as a Kalman filter. In [1, 2, 3] it was proved that the complementary filter is much simpler to calculate, so the energy consumption when using such algorithms is lower, which is critical for systems and devices running on batteries. Filters based on such algorithms allow you to fully assess the orientation of the UAV, using only data from the accelerometer and gyroscope. However, the filter fails when the dynamics of the UAV is large enough, and the output power of the accelerometer no longer provides a good estimate of the gravitational direction.

Currently, the problem of finding systems for determining the orientation of a moving body on the basis of complementary filters, or in a broader sense - on the basis of complexing meters is very relevant. In particular, the problem of synthesis of a complex system of discrete type is urgent.

Scientific and technical results. Synthesis of a discrete complement filter. We have the following general equation of the output angle for the orientation determination system based on a complementary filter of the analog type:

$$\hat{\gamma} = \gamma_1 + \gamma_2 = \frac{1}{Ts+1}\left[T(s\gamma + \delta_1) + \gamma + \delta_2\right] = \gamma + \frac{T}{Ts+1}\delta_1 + \frac{1}{Ts+1}\delta_2$$

And system error $\delta = \frac{T}{Ts+1}\delta_1 + \frac{T}{Ts+1}\delta_2$, which will not contain an infinitely increasing component of gyroscope drift. In addition, there will be a reduction in high-frequency noise of the gyroscope and accelerometer.

Consider now a discrete complementary filter. Let's write it down $\hat{\gamma} = \frac{1}{Ts+1}(TG + A)$ or $T\dot{\hat{\gamma}} + \hat{\gamma} = TG + A$. These equations define the equations of the analog filter. To switch from analog to discrete filter, write it down $\dot{\hat{\gamma}} = \frac{\hat{\gamma}(n) - \hat{\gamma}(n-1)}{\tau}$, τ – sampling time.

We obtain the equation of the discrete complementary filter:

$$\hat{\gamma}(n) = \left(1 - \frac{\tau}{T}\right)\hat{\gamma}(n-1) + \tau\left[G(n) + \frac{1}{T}A(n)\right] .$$

Note that, if necessary, you can synthesize a complementary filter, astatic relative to the drift of the gyroscope. We accept the transfer function W(s) as: $W(s) = \frac{a_2 s+1}{a_1 s^2 + a_2 s+1}$, than $1 - W(s) = \frac{a_1 s^2}{a_1 s^2 + a_2 s+1}$, obtaining the final scheme of the complexing filter in Fig.1-a:

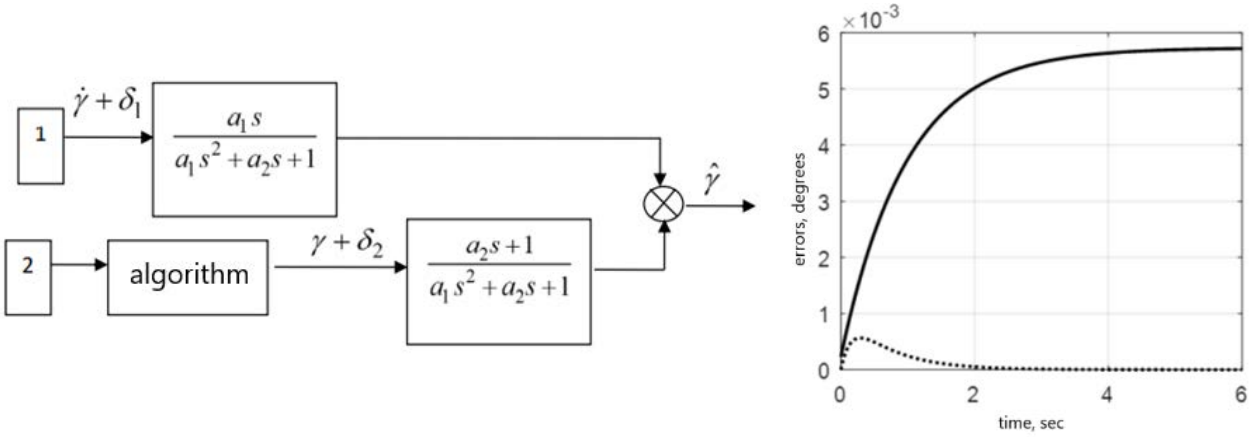

Fig.1-a the final scheme of the complexing filter (discrete); b - errors in calculating the angle

Then the resulting angle can be found as:

$$\hat{\gamma} = \gamma + \frac{a_1 s}{a_1 s^2 + a_2 s + 1}\delta_1 + \frac{a_2 s + 1}{a_1 s^2 + a_2 s + 1}\delta_2 \ .$$

Modeling of a complex system. Figure 1-b shows the errors in calculating the angle for $\delta_1 = 1 * 10^{-4} 1/c$ when using a filter with a transfer function $W(s) = \frac{1}{Ts+1}$, where T=1 sec (solid curve), and when using a filter with a transfer function $W(s) = \frac{a_2 s+1}{a_1 s^2+a_2 s+1}$ where $a_1 = 0.8 sec^2$; $a_2 = 0.1 sec$ (dashed curve).

Conclusion. The different range of measurements allows to significantly reduce the impact of these interferences on the accuracy of measuring angles by choosing corrective links. a wide range of complex circuits allows you to synthesize any system. The synthesis of the complementary filter of analog type is carried out and, accordingly, the synthesis-transition of the complementary filter of discrete type from the complementary filter of analog type is carried out. The use of CF is an effective means of eliminating the influence of gyroscope drifts on the accuracy of orientation.

References:

1. R. Zhu, D. Sun, Z. Zhou, and D. Wang, “A linear fusion algorithm for attitude determination using low cost mems-based sensors,” Measurement, vol. 40, no. 3, pp. 322–328, 2007.

2. R. Munguia and A. Grau, “Attitude and heading system based on ekf total state configuration,” in 2011 IEEE International Symposium on Industrial Electronics. IEEE, 2011, pp. 2147–2152.

3. J. L. Crassidis and F. L. Markley, “Unscented filtering for spacecraft attitude estimation,” Journal of guidance, control, and dynamics, vol. 26, no. 4, pp. 536–542, 2003.

UDC 629.735.33

Surkov K., Marynoshenko O.

LONGITUDINAL DYNAMICS IDENTIFICATION OF SMALL FIXED-WING UAV

Introduction. Unmanned aerial vehicles (UAVs) are extremely popular not only in military and civil applications, such as reconnaissance, mapping and agriculture, but also for scientific applications. One of the main fields of science, where UAVs and other drones are applied, is control system engineering. UAVs are much smaller, cheaper and easier to handle in comparison with full-scale aircraft, but at the same time could provide much more reliable results then the most complicated computer modeling due to real atmospheric disturbances. It is also worth to admit, that autonomous UAVs are much more reliable then simple RC aircrafts because modern autopilots such a Pixhawk with Ardupilot software are pretty reliable and redundant and in most cases human error is excluded.

The main objective of this research is to develop practical procedures for modelling and identification the flight dynamics of the small UAV. In the following paragraphs, the identification of the UAV “FLIRT Cetus” (developed by Abris Design Group [1] and shown in Figure 1) will be conducted. Cetus is a professional tool for aerial mapping, surveying and many other applications. Main geometry, mass and flight characteristics are shown in the Table 1 below.

Table 1. Main characteristics

Normal TOW, kg	9.9
Wing span, m	2.72
Length, m	1,1
Range of operational airspeeds, m/s	17...30
Flight time, min	up to 180

Figure 1. UAV Flirt Cetus

Cetus is a conventional fixed-wing airplane with flaperons (flaps mode wasn’t used during analysis) and rudder with elevator combined on the V-tail. UAV is powered by an electric power plant with 3-bladed folding fixed-pitch prop. More information can be found in [1].

The UAV is equipped with Pixhawk Cube autopilot, and navigation GNSS module. These modules have a lot of different MEMS sensors, that

provide measurements of angular rates, accelerations, barometric altitude, position, etc..

Scientific and technical results. In order to obtain a precise dynamic model of the UAV, a large number of flight experiments in different UAV configurations were conducted. Difference in wing span, TOW, cruise airspeeds were made in order to obtain more precise data about aerodynamic characteristics of individual parts of the UAV (such as wing, V-shaped stabilizer, fuselage, etc.). Flight data stored in .log files then were converted into Matlab data format and post processed. All flights have taken place during the sunset, when there is minimum thermal activity and wind is weak and stable. The final flight experiment, which results will be used for UAV identification was conducted with following UAV configuration:

Table 2. UAV configuration

TOW, kg	9.85
Wing span, m	2.72
Range of airspeeds, m/s	20...30
Airspeed step, m/s	1
Moment of inertia I_x , kg m^2	1.544
Moment of inertia I_y , kg m^2	1.7
Moment of inertia I_z , kg m^2	2.14
Moment of inertia I_{xz} , kg m^2	0.17

In addition, ground static tests of the powerplant were conducted in order to obtain a relationship between control signal (PWM) and static thrust of the motor with propeller (Fig.2). This data is recalculated with consideration of airspeed by the methods, described in [2] and used for inflight forces identifications.

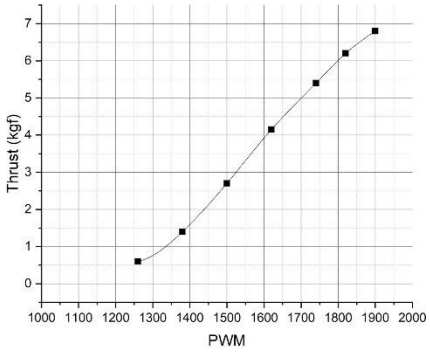

Figure 2. Thrust in flight and airspeed

For our purpose, only the first 30 minutes of flight will be taken into the research process. Time interval between data points is 0.1s. Some flight parameters are described on the diagrams below.

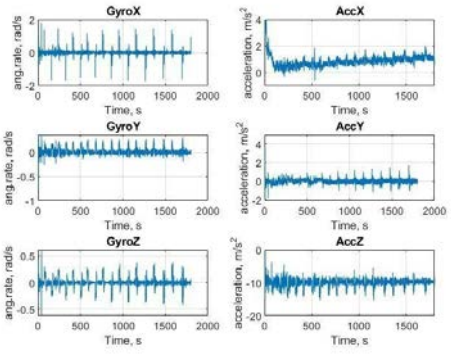

Figure 3. IMU data

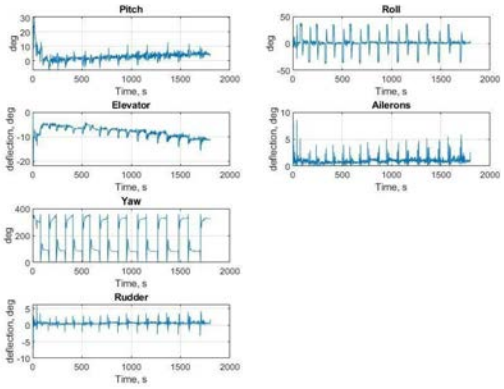

Figure 4. Attitude and control surfaces deflection

Control derivatives, that describe dependency between control surfaces deflections and force/moments generated we are considering as “known”, because they can be obtained with CFD analysis or approximately be calculated via standard aerodynamics methods. Our goal is to calculate stability derivatives, that are described in [3] and [4].

At the same time, longitudinal stability derivatives Y^{α} and M^{α} are already known, because they are very important during UAV development and essentially were used by aerodynamicists during the initial design process. Using the methodology described in [5] we will be looking for the absolute change in the forces magnitude.

It's worth mentioning that we don’t have AoA sensor onboard. In most other papers, constant speed is an important parameter and for this airspeed aerodynamically balanced state is taken into consideration. But in our case we have flight on different airspeeds and as a result at different balances states. That is the reason we are interested just in changes of flight parameters. We need to make some approximations for the future calculations.

1. Unsteadiness of the atmosphere causing just the changes in forces applied to the center of mass and not causing any moments.
2. Due to high flight time, high amount of data timepoints and large covered distance during the flight, external occasional influence of the air can be neglected.
3. Due to small time steps between data points, changes in AoA roughly equals changes in pitch angle $\Delta\alpha \approx \Delta\Theta$ due to inertia of the aircraft.
4. All calculations are made in a UAV-fixed frame of reference.

Knowing the acceleration data and pitch angle, we can calculate the additional force ΔY at any moment of time as follows:

$$mg = ma + Y_0$$

де Y_0 - normal force in balanced state

$ma = \Delta Y$ - increase of normal force, where:

$$\Delta Y = \Delta Y^{da}_{wing} + \Delta Y^{da}_{fuselage} + \Delta Y^{da}_{HS} + \Delta Y^{de}_{HS}\ \Delta Y^{d\delta\_elev}_{HS} + \Delta Y_P + \Delta Y^q$$

ΔY^{da}_{wing} - wing normal force gain component from the AoA changes

$\Delta Y^{da}_{fuselage}$ - fuselage normal force gain component from the AoA changes

ΔY^{da}_{HS} - horizontal stabilizer normal force gain component from the AoA changes

ΔY^{de}_{HS} - horizontal stabilizer normal force gain component from the wing downwash angle changes

$\Delta Y^{d\delta\_elev}_{HS}$ - horizontal stabilizer normal force gain component from the angle of elevator deflection changes

ΔY_P - normal force gain component from the thrust changes

ΔY^q - normal force gain component from the pitch angular velocity

The same equation can be formed for longitudinal moment:

$$\Delta M = \Delta M^{da}_{wing} + \Delta M^{da}_{fuselage} + \Delta M^{da}_{HS} + \Delta M^{de}_{HS}\ \Delta M^{d\delta\_elev}_{HS} + \Delta M_P + \Delta M^q$$

By normalizing forces equations by $\rho V^2 S/2$ and moment equations by $\rho V^2 Sb/2$ we can work with derivatives and coefficients. Most of these parameters are simple to calculate, but wing downwash angle is not that simple. We can calculate this angle for every point of horizontal stabilizer as shown in [6] and then integrate the distribution obtained.

Solving this system for Cy^q and mz^q in every time point, we are obtaining results in which air disturbances are included. Taking into account considerations mentioned above, by calculating the average magnitude of the derivatives, we are excluding air disturbances and obtaining, that $Cy^q = 13.64$, $mz^q = -6.092$.

References:

1. Abris Design Group https://abris.aero/
2. Chumak, P. Krivokrisenko, V. *"Calculation, design and construction of ultralight aircraft"*
3. Klein, V. and Morelli, E. A., *Aircraft System Identification: Theory and Practice,* AIAA, Reston, VA.
4. Andrei Dorobantu , Austin M. Murch, Bernie Mettler, and Gary J. Balas *Frequency Domain System Identification for a Small, Low-Cost, Fixed-Wing UAV*
5. Howard Loewen *"Stability derivatives. What they are and how they are used"*
6. Yuryev, B.N. *Experimental aerodynamics*[in 2 parts.]/ Part 2 : *Theoretical basics of experimental aerodynamics.* 1936.

UDC 623.4:623.5

Vandio O., Sukhov V.

INFLUENCE OF DESIGN PARAMETERS OF A STEALTH ROCKET ON VISIBILITY

Introduction. First ideas and prototypes of cruise missile armor:

- In 1907 Sci-fi film with “air torpedo”
- Pilotless fighter in late 1920th in UK
- V-1 German cruise missile the first working CM ever

How we use cruise missiles today and what makes them so efficient armor?

What cruise missiles stealth consist of?

- Radio-absorbing coating
- Specific body shape allow to reduce RCS (Radar cross-section)

Specific of stealth technologies for cruise missiles that makes it deferent from fighters, bombers, UAVs etc. What is the main specific feature of cruise missile? – altitude. Extremely low altitude.

How does low altitude works? How it affect on stealth characteristics and should we do with that? Modern missiles is a new generation of armor – they are smart. They fly without human control and can decide witch trajectory to choose to get the maximum chance of enemy defeat.

Modern battleships and some state military objects (storages, bases, fortifications etc) are the most common targets for CM. So for defending them people uses many of applications against CM and aviation, but they always uses locators to detect danger before it comes. We often name that locators radars. Stealth technologies should make FO (flying objects) invisible for radars.

Scientific and technical results. Low altitude is used to hide CM behind the horizon. Where is problem? – Problem can be at the place where altitude of CM is high. Where is the highest point of trajectory during all CM flight? – At the start, or to be more true after the start.

Describing the scheme of launching cruise missile.

Stage 1 – velocity and altitude raise due to launching engine work

Stage 2 – inertial flight with raising altitude and reducing velocity

Stage 3 – inertial straight flight with reducing velocity

Stage 4 – sailing flight, velocity= constant, altitude decries

Stage 5 – transition to cruise flight with started engine

How to do how maximum altitude during launch affect on stealth characteristics? Describing graph of detecting length and apogee altitude. How to explore the launching trajectory? Method of modeling starting trajectory. Describing the method of modeling launching trajectory its mathematics and etc.

How Missile oscillate during launch? What affect on missiles oscillations? How to calculate oscillations?

So now we can get a mass of trajectories that are based on difference in

starting conditions and also calculate oscillations on each of them. We also can analyze that oscillations and answer the question :'can CM exist on that trajectory or not'?. So we can choose the best trajectory for cruise missile.

Conclusion. What would we get if uses best trajectory?

- We will increase launching safety.
- We will save radar invisibility.
- Increase chances of successful attack.

UDC 629.7.05

Vovk Y. E., Ponomarenko S. O.

INTEGRATED NAVIGATION COMPLEX OF UNMANNED AIRCRAFT ON THE BASIS OF SATELLITE AND COURSE-AIR INFORMATION

Introduction. To ensure the required accuracy and reliability of operation in conditions of interference as on-board systems for calculating the coordinates of unmanned aerial vehicles (UAVs) are used inertial and course-air systems. Given the rigid mass and dimensional constraints on the payload, the airborne system has certain advantages for small UAVs, for which, in contrast to the inertial system, there is a linear nature of the increase in errors in the calculation of coordinates over time. The on-board equipment (BA) of the satellite navigation system (SNA) is also used in the UAV navigation complex, which, under normal operation, provides high-precision positional-speed correction of the coordinate numbering system.

To develop an algorithm for complex processing of navigation information from course-air sensors of UAVs (air speed sensor, barometer, three-component magnetometer, sensors of pitch, roll, attack and slip) and BA SNA.

Scientific and technical results. Taking into account the results presented in [1, 2, 3], the following navigation equations for the given coordinates R_N (t) and R_E (t) can be used in the course-aerial calculation of the coordinates of the UAV location with acceptable accuracy for practice:

$$\dot{R}_N(t) = V_N(t)\, C_1[\varphi(t), h(t)];$$

$$\dot{R}_E(t) = V_E(t)\, C_2[\varphi(t), h(t)], \qquad (1)$$

where

$$R_N(t) = [\varphi(t) - \varphi_П]\, R_3;$$

$$R_E(t) = [\lambda(t) - \lambda_П]\, R_3; \qquad (2)$$

$$C_1[\varphi, h] = \frac{R_3}{a}\,[1 + e^2\,(1 - 1{,}5\sin^2\varphi(t)) - h(t)/a]; \qquad (3)$$

$$C_2[\varphi, h] = \frac{R_3}{a\cos\varphi(t)}\,[1 + 0{,}5e^2\sin^2\varphi(t) - h(t)/a];$$

φ (t), λ (t) - latitude and longitude; - flight altitude above the surface of the terrestrial ellipsoid; $\varphi_П$, $\lambda_П$ - coordinates of the set point in the area of flights; R_3 - is a constant taken equal to the radius of the earth's sphere;

V_N (t), V_E (t) - projections of the UAV path speed on the horizontal axes of the geographical triangle; a, e^2 - the major half-axis and the square of the eccentricity adopted for navigation of the terrestrial ellipsoid.

The current components of the road speed V_N (t), V_E (t) satisfy the following ratio:

$$V_N(t) = V_{\text{ПОВІТ } N}(t) + V_{\text{ВІТРУ } N};$$

$$V_E(t) = V_{\text{ПОВІТ } E}(t) + V_{\text{ВІТРУ } E} \quad (4)$$

where $V_{\text{ПОВІТ } N}$ (t) and $V_{\text{ПОВІТ } E}$ (t) are projections of the UAV air velocity on the N and E axes;

$V_{\text{ВІТРУ } N}$ and $V_{\text{ВІТРУ } E}$ are the horizontal components of wind speed.

In the General case, the expressions for the horizontal components of air speed have the form [4]:

$$V_{\text{ПОВІТ } N}(t) = V_{\text{ПОВІТ}}(t)\{\cos\vartheta(t)\cos\psi_{\text{И}}(t)\cos\alpha(t)\cos\beta(t)+[\sin\psi_{\text{И}}(t)\sin\gamma(t)+\cos\psi_{\text{И}}(t)\cos\gamma(t)\sin\vartheta(t)]\sin\alpha(t)\cos\beta(t)+[\cos\psi_{\text{И}}(t)\sin\vartheta(t)\sin\gamma(t)-\sin\psi_{\text{И}}(t)\cos\lambda(t)]\sin\beta(t)\}$$

$$V_{\text{ПОВІТ } E}(t) = V_{\text{ПОВІТ}}(t)\{\cos\vartheta(t)\sin\psi_{\text{И}}(t)\cos\alpha(t)\cos\beta(t)+[\sin\psi_{\text{И}}(t)\sin\vartheta(t)\cos\gamma(t)-\cos\psi_{\text{И}}(t)\sin\gamma(t)\sin\alpha(t)]\cos\beta(t)+[\cos\psi_{\text{И}}(t)\sin\gamma(t)+\sin\psi_{\text{И}}(t)\sin\vartheta(t)\sin\gamma(t)]\sin\beta(t)\} \quad (5)$$

where $V_{\text{ПОВІТ } N}$ (t) is the current air speed; $\psi_{\text{И}}$ (t), ϑ(t), γ(t) - current angles of true course, pitch and roll; α (t), β (t) - current angles of attack and slip.

Angles of attack and slip can be determined by an indirect method based on measurements of UAV accelerations and a priori information about the coefficients of aerodynamic forces by the following formulas [8]:

$$\alpha = -(a_{y1}/a^*_{x1}K_0)(1 + a^{\alpha}_{y}/a_x)^{-1};$$

$$\beta = -a_{z1}/a^*_{x1}\ (1 + c^{\beta}_{z}/c_x)^{-1};\ (|\alpha| < 10^o,\ |\beta| < 10^o); \quad (6)$$

$$a^*_{x1} = a_{x1} - \text{P/m},$$

where a_{x1}, a_{y1}, a_{z1} are the components of the acceleration determined by the accelerometers, which are installed on the connected axes near the center of mass of the UAV; P, m - thrust and mass of UAVs; c_{y0} , c_{x0} , $c^{\alpha}_{y} = \frac{\partial c_y}{\partial \alpha}$, $c^{\beta}_{y} = \frac{\partial c_z}{\partial \beta}$, $c_x = c_x(c_y)$ - aerodynamic coefficients; $K_0 = c_{y0}/c_{x0}$ is the aerodynamic quality of the UAV, which corresponds to the zero angle of attack ($\alpha = 0$).

Information about the current values of air speed, pitch angles and roll comes from the appropriate sensors. The current estimate of the true course angle is determined by the formula of the form:

$$\psi_{\text{И}}(t) = \psi_M(t), + \delta_M \quad (7)$$

where ψ_M is the value of the magnetic course; δ_M is the value of the magnetic declination.

In turn, to calculate the current estimate of the magnetic course uses a formula of the form: ψ_M (t)=arctg(- f_1 / f_2),

де $f_1 = Hy_1$ (t)sinγ(t) + Hz_1 (t)cosγ(t); (8)

$f_2 = Hx_1$ (t)sinϑ(t) - Hy_1 (t)cosϑ(t)sinγ(t) + Hz_1 (t)sinϑ(t)sinγ(t) ;

Hx_1 , Hy_1 , Hz_1 - current estimates of projections of the Earth's magnetic field vector on the axis of the coordinate system connected to the UAV, coming from a three-component magnetometer.

Initial data for mathematical modeling. The efficiency of the proposed algorithm for complexing course-air sensors and BA SNA was evaluated using mathematical modeling. The simulation set the motion of a small UAV at altitudes of 0… 1000 m with speeds of 40… 80 m / s on the trajectories of maneuvers such as "snake" and "circle" and used a simplified model of errors in measuring the true course, including systematic and random components. RMS values of errors of course-air sensors were set as follows: = 1 m / s; = 2 mrad; = 1 m; = 3 mrad, and the displacement of the sensor readings = ± 3 m; ± 30 mrad.

The root mean square values of positional and velocity errors of the SNA BA were taken as = 3 m; = 0.03 m / s.

The actual values of the horizontal components of the stationary wind speed in the area of flights varied within ± 20 m / s, and their initial estimates were set with errors of ± 15 m / s.

The step of processing navigation information was taken equal to 0.1 s, and the parameters of procedures (17) and (19): = 5 s, = 10.

The results of mathematical modeling. Using the regression procedure (17) for the first 50 seconds of flight, the correction to the course angle measurements was estimated with an error of not more than 3 mrad, and the correction to the initial estimates of the horizontal components of the steady wind speed - with errors of not more than 0.3 m/s.

To test the procedure (19), wind jumps with amplitudes of ± 15 m/s at given discrete moments of time were simulated. The revised corrections to the initial estimates of the wind speed components after the jumps were identified with errors of no more than 0.2 m/s.

Conclusion. Thus, the simulation results confirmed the efficiency and fairly high efficiency of the proposed modernized non-invariant compensation scheme for complexing course-air sensors and SNA BA for small UAVs.

UDC 629.7.02

Zakharchenko M., Kozei Y.

MINIMIZATION OF THE MASS FOR AERODYNAMIC CONFIGURATION "TANDEM"

Introduction. The study of the influence of the layout scheme of the fuselage of the ultralight aircraft of the aerodynamic scheme "tandem" on its aerodynamic, mass characteristics and strength was performed in this work.

The choice of a rational layout of the aircraft fuselage is an important stage of design.

The fuselage of the model is made according to the most common schemes: classic, single-beam and double-beam.

Minimizing the weight of the structure and ensuring sufficient strength and rigidity is one of the main tasks of designing any aircraft.

Aircraft that use solar energy for flight are characterized by low wing load and high aerodynamic quality values.

The "tandem" scheme has certain features and requirements for the fuselage. For example, the fuselage of the "tandem" circuit perceives more torque, it has a different mass distribution and more.

The purpose of this work is to study the influence of the layout of the fuselage of the ultralight aircraft of the aerodynamic scheme "tandem" on its aerodynamic mass characteristics and strength.

Scientific and technical results. In this study, a single-beam fuselage is characterized by a bow containing equipment and a power plant. And the fuselage has a tail beam that connects the front, rear wing and vertical plumage. The fuselage with two beams has a body which is characterized by a bow and two beams. They connect the wings and vertical plumage.

The process of this study can be divided into the following stages: the formation of geometric parameters, determination of aerodynamic characteristics, calculations of the mass of the structure, the calculation of strength, the study of stiffness.

The study of the layout of the fuselage was carried out under the condition of compliance with the same geometric characteristics of the aircraft. The main requirements for the fuselage are:

- optimal placement and operation of the payload;
- minimum aerodynamic drag;
- minimum weight;
- sufficient strength and rigidity.

Classic, single-beam and double-beam fuselages have a cross-sectional area of S_f. It has no round shape and it consists of a bow and a tail that combine wings and plumage. The main parameters are the length L_f, the diameter of the largest cross-sectional area or equivalent diameter d_f, elongation λ_f, maximum height H_f, maximum width B_f, beam diameter d_m.

Fuselage resistance consists of friction resistance, pressure resistance and impedance.

Frictional resistance is a significant part of the resistance at subcritical flight speeds. Its value is proportional to the surface area of the fuselage. Therefore, increasing the length of the fuselage at a given mid-sectional area (increasing elongation) leads to an increase in surface area.

For each layout of the aircraft, a purge was performed at a speed of 70 km/h using the Flow Simulation package.

The classic fuselage creates significant indicators of aerodynamic drag, friction resistance. Single-beam fuselage creates the lowest aerodynamic drag among the considered schemes under the same calculation conditions. The double-girder fuselage creates relatively low aerodynamic drag and friction drag.

Spatial models of fuselages are built and the materials from which they are made are indicated. as well as modeling of the glued joints of the fuselage components was carried out to determine the weight of the structure. Larit L-285 epoxy resin was used for joints.

The classic fuselage has significant mass values at the same dimensions and load. Single-beam fuselage has the lowest value of mass. The double-girder fuselage has a relatively small mass at similar dimensions and loads.

The distance between the front and rear wings has the most significant impact on the stiffness characteristics of the fuselage. The dependence of the influence of the distance between the wings of the aircraft on the value of the maximum deformation Δh caused by the bending moment M_z, for each of the studied fuselage schemes is formed to assess the stiffness characteristics of the fuselage.

Strength calculations were performed in the APM FEM package for the COMPASS-3D and SOLIDWORKS 2016 programs.

Structural rigidity and deformation values are the best in the classic fuselage scheme. The rigidity of the structure and the value of deformation are the worst in the single-beam fuselage in comparison with other studied schemes. The rigidity of the structure and the deformation of the double-girder fuselage are acceptable.

Calculations have shown that the structures of the classic and double-girder fuselages can withstand the load acting on this type of aircraft in flight. And the single-girder structure needs reinforcement at the junction of the beam and the bow. This will negatively affect the mass figures.

The analysis of the obtained results allows to form a list of advantages and disadvantages of the studied fuselage schemes; it also allows to determine the areas of application of each scheme.

The results of the calculations of aerodynamic characteristics showed that the junction of the fuselage, plumage and rear wing creates a zone of turbulence

in all models. This adds an additional component to the indicative resistance and it also impairs the efficiency of the plumage.

Small values of mass and aerodynamic drag have a positive effect on energy consumption for the flight and its duration.

Low values of structural rigidity will lead to deterioration of controllability and stability in flight together with the center of mass shifted to the bow.

Conclusions. Therefore, it is established that a rational solution is the use of a two-beam fuselage layout scheme for the implementation of the design of aircraft with low specific gravity (for example, aircraft with solar energy).

The double-girder fuselage creates relatively low indicators of aerodynamic resistance, weight of a design at identical dimensions and loading conditions. This helps to reduce the energy consumption of the flight and increases its duration. In this case, the rigidity of the structure is acceptable and it does not significantly affect the stability and controllability of the aircraft.